J. Phys. B: At. Mol. Opt. Phys. **32** (1999) 2415–2431. Printed in the UK PII: S0953-4075(99)00027-9

Elastic and vibrationally inelastic slow collisions: $H + H_2$, $H^+ + H_2$

Predrag S Krstić and David R Schultz
Physics Division, Oak Ridge National Laboratory, Oak Ridge, TN 37831-6373, USA

Received 9 December 1998

Abstract. We report on a comprehensive study of the scattering of hydrogen atoms on the ground electronic surface of hydrogen molecules in the range of centre of mass energies 0.1–100 eV. Differential and integral elastic cross sections, the related transport cross sections, and vibrationally inelastic cross sections starting from both ground and excited vibrational states, are calculated using a fully quantal, coupled-channel approach in a truncated vibrational basis set, while the rotational dynamics of H_2 is treated with the infinite order sudden approximation prescription. For comparison and to highlight the major physical mechanisms revealed in these collisions, a parallel study is carried out for scattering of protons on hydrogen molecules.

1. Introduction

Recent interest in earlier work on elastic collisions between both charged and neutral particles with neutral constituents of relatively cold ($\sim$1–10 eV) hydrogen plasmas has been revived by the need to establish a full description of the neutral gas transport in the boundary of tokamak plasmas, such as in the divertor and edge plasma regions [1, 2]. For example, spreading the heat load, recycling hydrogen, and removing the helium ash and impurities are basic functions of the divertor and are critical for engineering magnetically confined plasma fusion devices. In the cold and high-density plasma characterizing these regions, elastic scattering plays by far the dominant role in momentum transfer and particle transport due its correspondingly large cross section. In addition to the integral and differential elastic cross sections needed to model these processes, rate coefficients (cross sections averaged over the Maxwellian temperature distributions) are needed, so we consider the somewhat extended centre of mass energy region of 0.1–100 eV in what follows, and utilize atomic units except where explicitly noted.

At least in principle, the particles of interest include hydrogen ions (H^+, D^+, T^+), atoms (H, D, T), and molecules (H_2, D_2, DT, ...) as well as ions and atoms of helium and intrinsic (e.g. C, Be, B) and extrinsic (e.g. Li, Ne, Xe) impurities. Elastic neutral–neutral collisions have been the least studied among these, while the data for scattering from molecular systems are almost entirely unavailable. To our knowledge, only one comprehensive set of data is available for the latter over an extended energy range (0.067–6670 eV). This data is in the form of the momentum transfer cross section for $H + H_2$ collisions found by Phelps [3] through interpolation of experimentally derived data at low energies up to theoretical results (Smith *et al* [4]) at high energies. However, a certain amount of data is available at temperatures lower than those of present interest [5] regarding in particular rotational excitations needed for interpretation of the infrared emission and cooling of interstellar clouds. In contrast, the $H^+ + H_2$ collision system has been often studied, but not in a comprehensive manner, being

0953-4075/99/102415+17$19.50 © 1999 IOP Publishing Ltd

the most fundamental and simplest ion-molecule system [6–15] from sub-eV to keV energies, with regard to elastic scattering, rotational and vibrational excitation, and charge transfer.

The $H^+ + H_2$ charge transfer reaction, although endoergic, has a low threshold energy (1.83 eV), and is strongly coupled to the mechanism of vibrational excitation to states that are high enough ($v \geqslant 4$) to overcome the barrier. Thus, this reaction is a second-order process with integral cross section that is more than ten times lower than the cross section for excitation to the first vibrationally excited state of H_2 for energies <200 eV [3]. On the other hand, in order for the electron to make a transition to the excited surface ($H + H_2^+$) the H_2 bond must stretch while the projectile is still close enough to the H_2 molecule. Collisions that involve nuclear rearrangements will almost always lead to scattering at larger angles which will not significantly contribute to the presently considered elastic cross section results, but could influence to some extent the transport cross sections due to their emphasis of large angle scattering. Thus, in the energy range considered here, it is satisfactory to treat elastic scattering and vibrational excitations with inclusion of only the ground electronic energy surface with the appropriate caution (i.e. using the transformation to the diabatic surface in the $H^+ + H_2$ case). This is the first assumption made in the present calculations. Moreover, the energy gap for any reaction that involves an electronic transition is much larger for neutral–neutral collisions, which allows greater certainty in the results obtained with only one electronic surface.

The second simplifying approximation is a variation of the so-called sudden approximation known as infinite order sudden approximation (IOSA) [6, 7, 16, 17]. When the rotational motion is adiabatic with respect to the relative translational motion of the molecule and a colliding particle, the projectile effectively interacts with a molecule that has no rotational angular momentum. Such a physical situation allows the complete decoupling of the diatomic rotational and projectile orbital angular momenta in the scattering system and leads to an enormous simplification in the equations of motion. Hence, the rotationally summed cross sections only depend on the initial ground rotational state. The Hamiltonian contains only a vibrational kinetic energy operator as a 'signature' of the molecular target, but also depends parametrically on the molecular orientation which is fixed during the collision. The calculations need to be repeated for a range of orientations and the resulting cross sections averaged. This approach has been followed for both fully quantal and semi-classical formulations and has been shown to be strictly valid only for systems with short-range rotational coupling. Thus the sudden approximation is most applicable to the neutral–neutral system ($H + H_2$) where the anisotropy of the interaction is short-ranged.

Specifically, we have used the IOSA over the whole energy range considered and found that it suffices to expand the wavefunction in a truncated basis of nine vibrational states. For $H^+ + H_2$ this allows convergence of the results for at least three excited states and five for $H + H_2$. However, for ion–molecule systems additional caution is needed since the sudden approximation is expected to be valid for the $H^+ + H_2$ system above a collision energy of about 3 eV [12], while for lower energies its validity remains undetermined due to the lack of more elaborate calculations or measurements. Nevertheless, since typical rotational energies for H_2 are of the order of 0.01 eV or less, the classical argument of freezing molecular rotations for the duration of the collision for $E > 0.1$ eV indicates that acceptable results may be obtained as long as rotationally averaged cross sections are calculated.

Some of the existing calculations for $H^+ + H_2$ collisions utilize the 'time-dependent' or 'impact parameter' formalism which assumes a classical or often straight-line motion of the projectile [13]. While the straight-line trajectory method could be an acceptable approximation for small scattering angles, it poorly describes the scattering at larger angles. As demonstrated below, the scattering angles following vibrational excitation for both proton and neutral atom impact are shifted significantly toward larger values in comparison with the behaviour displayed

by elastic scattering. Thus we chose a fully quantal approach for both the projectile and diatomic vibrational motion, the details of which are given in section 2.

We present and discuss the results of these calculations in section 3. In particular, differential and integral elastic and transport cross sections are shown for $H + H_2$ and $H^+ + H_2$ collisions, for both ground and vibrationally excited states, and compared with relevant existing data. The cross sections for vibrational excitation of several low-lying excited states are also shown. It turns out that the principal mechanism for this process in the $H^+ + H_2$ system is well understood [10] and is mainly an effect of 'bond dilution'—the temporary depletion of electron density from the molecular bond by the passing proton. The vibrational excitation is caused by the stretching force which acts simultaneously on both of the H_2 nuclei. This becomes significant at small distances, thus causing the largest contribution to the cross section for large scattering angles. This mechanism is apparently weaker in $H + H_2$ scattering and the incident atom interacts predominantly with the nearest atom of the molecule. This is elucidated below through comparison with the elastic cross sections in the H+H system, as well as with the dependence on the molecular orientation. Overarching conclusions regarding the present systems are given in section 4. We note here that all collision energies and scattering angles used are given in the centre of mass system.

2. Theoretical framework

We have calculated the elastic differential and integral (elastic, momentum transfer, viscosity) cross sections for scattering of protons and hydrogen atoms from H_2 on the ground electronic and vibrational ($\nu = 0$) state as well as on the excited ($\nu = 1, 2, 3$) vibrational states. Inelastic cross sections for vibrational excitation on the ground electronic surface were also computed. Inelastic processes that involve a change of electronic molecular state were neglected as discussed in section 1.

Specifically, we treat collisions of the type

$$\begin{aligned} H^+ + H_2(\nu_i) &\rightarrow H^+ + H_2(\nu_f) \\ H + H_2(\nu_i) &\rightarrow H + H_2(\nu_f) \end{aligned} \tag{1}$$

where $\nu_{i,(f)}$ denotes the initial (final) vibrational state of H_2. Although these are among the simplest of all ion/atom–molecule collisions, an *ab initio* numerical solution of the problem is an extremely difficult computational task. This is mainly due to the difficulty in handling the large manifold of ro-vibrational degrees of freedom in the target molecule as well as in accounting for the presence of reactions with interchange of particles.

The approximations that can make the computation tractable depend on the process to be considered as well as on the collision energy range. For example, in the range above a few hundred eV, the projectile is so fast that both the internuclear diatomic coordinate and its direction in space may be considered as frozen during the collision. This significantly simplifies the treatment of the collision dynamics of the electronic transitions, resulting in methods similar to those employed to treat ion–atom or atom–atom collisions. In contrast, consideration of the collision energies below 100 eV, down to about 1 eV, requires simultaneous coupling of the electronic and vibrational motions. In particular, the excitation energy of the first vibrational state of H_2 is $\sim$0.5 eV corresponding to a characteristic vibration time exceeding 50 au which is comparable to the collision time for energies $\sim <$100 eV. As we have noted above, the collision time is still short enough on the scale of molecular rotations (excitation energy $<$0.01 eV, i.e. the characteristic times $\sim >$3000 au), thus enabling one to consider the direction of the diatomic internuclear axis as fixed (IOSA). The pertinent angle, γ, is defined as the angle between the reaction coordinate $\vec{R}$ (from the centre of mass of the H_2 molecule to the projectile nucleus)

with the diatomic internuclear axis $\vec{\rho}$. But since the adiabatic triatomic molecular surfaces on which the collision dynamic evolves at these energies is not isotropic with respect to γ, especially at small internuclear distances, one needs to calculate the observables for different angles γ and then average over them. As discussed in the introduction, for a particular initial and final vibrational state this is equivalent to the summation over all final, and average over initial, rotational states.

The total Hamiltonian of the problem can be written in terms of the nuclear kinetic energy operator T_{N} and electronic energy operator $\mathcal{H}_{\mathrm{e}}$

$$\mathcal{H} = T_{\mathrm{N}} + \mathcal{H}_{\mathrm{e}}. \tag{2}$$

Using the Born–Oppenheimer prescription for separation of the fast electronic and slow nuclear motions, one expands the wavefunction in terms of a complete set of eigenfunctions $\Phi_k(\vec{r}, \{\vec{R}_{\mathrm{N}}\})$ of the electronic Hamiltonian for fixed $\{\vec{R}_{\mathrm{N}}\}$ as

$$\Psi = \sum_k f_k(\{\vec{R}_{\mathrm{N}}\})\Phi_k(\{\vec{r}\}, \{\vec{R}_{\mathrm{N}}\}) \tag{3}$$

where $\{\vec{r}\}$ and $\{\vec{R}_{\mathrm{N}}\}$ are the sets of electronic and nuclear coordinates, respectively, and summation also implies integration over the electronic continuum. Substituting equation (3) into the Schrödinger equation for the problem yields a set of coupled partial integro-differential equations for the 'nuclear' amplitudes f_k

$$\sum_k H_{jk} f_k + [T_{\mathrm{N}} + E_j(\{\vec{R}_{\mathrm{N}}\}) - E] f_j = 0 \tag{4}$$

where E_j are eigenenergies of the electronic Hamiltonian, E is the total (conserved) energy of the colliding system and H_{jk} are matrix elements of the dynamic (nonadiabatic) interaction having the structure

$$H_{jk} = -\frac{1}{2}\sum_{N_i}\left\langle \Phi_j \left| \frac{\nabla^2_{N_i}}{m_{N_i}} \right| \Phi_k \right\rangle - \sum_{N_i}\left\langle \Phi_j | \frac{\vec{\nabla}_{N_i}}{m_{N_i}} | \Phi_k \right\rangle \cdot \vec{\nabla}_{N_i} \tag{5}$$

where summation is taken over the set of nuclei $\{N_i\}$ with masses m_{N_i} and $\vec{\nabla}_{N_i}$, $\nabla^2_{N_i}$ are the gradient and Laplacian operator for a nuclear coordinate $\vec{R}_{N_i}$.

For an ion (or atom) scattering from a diatomic molecule the set of nuclear coordinates may be chosen in terms of the diatomic internuclear separation ρ, the internuclear separation of the ion (or atom) and the diatomic centre of the mass, $\vec{R}$, and the angle γ between $\vec{R}$ and $\vec{\rho}$. For a fixed γ (IOSA) T_{N} simplifies significantly. That is, this yields for the kinetic energy part of the radial equation the form [7]

$$T_{\mathrm{N}}^{(\ell)} = -\frac{1}{2M}\frac{\partial^2}{\partial R^2} - \frac{1}{2\mu}\frac{\partial^2}{\partial \rho^2} + \frac{1}{2M}\frac{\ell(\ell+1)}{R^2} \tag{6}$$

where M and μ are the reduced masses of the three-atom and diatomic molecule, respectively, and ℓ is the angular momentum quantum number of the relative projectile–molecule motion. The absence of a diatomic centrifugal energy term is one of the peculiarities of the IOSA.

In order to solve the problem defined above we expand the partial waves $f_k^{(\ell)}$ of the nuclear wavefunctions for each electronic state k in the full set of vibronic wavefunctions $\lambda_\nu^{(k)}(\rho)$, (with $\varepsilon_\nu^{(k)}$ the corresponding eigenvalue), i.e.

$$\left(-\frac{1}{2\mu}\frac{\partial^2}{\partial \rho^2} + E_k(R \to \infty, \rho)\right)\lambda_\nu^{(k)}(\rho) = \varepsilon_\nu^{(k)}\lambda_\nu^{(k)}(\rho). \tag{7}$$

We note that $E_k(R, \rho, \gamma)$ for finite R does not depend on γ when the projectile is far enough from the diatom, that is, the adiabatic potential is isotropic in that limit. Therefore, with the ansatz

$$f_k^{(\ell)}(R, \rho, \gamma) = \sum_\nu a_\nu^{(k,\ell)}(R, \gamma)\lambda_\nu^{(k)}(\rho) \tag{8}$$

using equations (6) and (4) yields

$$\left[-\frac{1}{2M}\frac{\partial^2}{\partial R^2} + \frac{1}{2M}\frac{\ell(\ell+1)}{R^2} - (E - \varepsilon_\nu^{(j)})\right] a_\nu^{(j,\ell)} + \sum_\mu W_{\nu\mu}^{(j)}(R, \gamma)a_\mu^{(j,\ell)} + \sum_{\mu,k} H_{jk}^{(\nu,\mu)}(R, \gamma)a_\mu^{(k,\ell)} = 0 \tag{9}$$

where

$$W_{\nu\mu}^{(j)}(R) = \langle \nu | E_j(R, \rho, \gamma) - E_j(R \to \infty, \rho) | \mu \rangle \tag{10}$$

and

$$H_{jk}^{(\nu,\mu)}(R, \gamma) = \langle \nu | H_{jk}(R, \gamma, \rho) | \mu \rangle \tag{11}$$

for all electronic states j, and all vibrational states ν. This system of ordinary differential equations is extremely difficult to solve, not so much because of its size, but rather due to the difficulties in accurately determining all of its matrix elements. Besides, it has to be solved for each orientation angle γ, since the cross sections are to be averaged over it.

With the single electronic surface and IOSA prescriptions the final form of the system of coupled, second-order differential equations follows as

$$\left[-\frac{1}{2M}\frac{\partial^2}{\partial R^2} + \frac{1}{2M}\frac{\ell(\ell+1)}{R^2} - (E - \varepsilon_\nu)\right] a_\nu^{(\ell)} + \sum_\mu W_{\nu\mu}(R, \gamma)a_\mu^{(\ell)} = 0 \tag{12}$$

where we omit the index of the electronic surface. This system of equations was solved numerically using Johnson's algorithm [19] of logarithmic derivatives for each angular quantum number ℓ and using the standard plane wave boundary conditions to construct the K-matrix and from it, the S-matrix.

Once the S-matrix is found the differential cross section for a transition into vibrational state (ν_f) is [7]

$$\frac{\mathrm{d}\sigma^{\nu_\mathrm{f},\nu_\mathrm{i}}(E, \theta)}{\mathrm{d}\Omega} = \frac{1}{8K^2}\sum_\ell \sum_{\ell'} (2\ell+1)(2\ell'+1)P_\ell(\cos\theta)P_{\ell'}(\cos\theta) \times \int_0^\pi \mathrm{d}\gamma\ \sin\gamma(\delta_{\nu_\mathrm{f},\nu_\mathrm{i}} - S_{\nu_\mathrm{f},\nu_\mathrm{i}}^{(\ell)}(\gamma))(\delta_{\nu_\mathrm{f},\nu_\mathrm{i}} - S_{\nu_\mathrm{f},\nu_\mathrm{i}}^{(\ell')*}(\gamma)) \tag{13}$$

where $\vec{K}$ is the initial projectile momentum, $\delta_{i,j}$ is the Kronecker symbol, $S_{\nu_\mathrm{f},\nu_\mathrm{i}}^{(\ell)}$ is the ℓth angular momentum component of the S-matrix for the transition from the initial (ν_i) to final (ν_f) vibrational state, and θ is the centre of mass scattering angle. Finally, the total cross section is obtained by integration over the full scattering solid angle Ω, which yields

$$\sigma^{\nu_\mathrm{f},\nu_\mathrm{i}}(E) = \frac{\pi}{2K^2}\sum_\ell (2\ell+1)\int_0^\pi \mathrm{d}\gamma\ \sin\gamma|(\delta_{\nu_\mathrm{f},\nu_\mathrm{i}} - S_{\nu_\mathrm{f}}^{(\ell)}(\infty, \gamma))|^2. \tag{14}$$

For the elastic channel, $\sigma_\mathrm{el}^{\nu_\mathrm{i}}(E) \equiv \sigma^{\nu_\mathrm{i},\nu_\mathrm{i}}(E)$, we also calculate the first two moments of the total elastic cross section which are of interest for plasma modellers (see e.g. [18]). These are the momentum transfer (diffusion) cross section

$$\sigma_\mathrm{mt}^{\nu_\mathrm{i}} = \int \mathrm{d}\Omega\, \frac{\mathrm{d}\sigma_\mathrm{el}^{\nu_\mathrm{i}}(E, \theta)}{\mathrm{d}\Omega}(1 - \cos\theta) \tag{15}$$

and viscosity cross section

$$\sigma_{\rm vi}^{\nu_i} = \int {\rm d}\Omega \, \frac{{\rm d}\sigma_{\rm el}^{\nu_i}(E,\theta)}{{\rm d}\Omega} \sin^2\theta. \tag{16}$$

The main contribution to the integral elastic cross section comes from the forward scattering angles. In contrast, $\sigma_{\rm mt}^{\nu_i}$ is dominated by the backscattering part of the differential cross section, since the weighting factor $(1-\cos\theta)$ is maximum at $\theta = \pi$. Since the change in momentum p of an elastically scattered particle is $p(1-\cos\theta)$, $\sigma_{\rm mt}^{\nu_i}$ is a measure of the average momentum lost in such a collision. The backscattering retards the diffusion of particles in a gas or plasma, and thus this loss of forward momentum determines the rate of diffusion. One can also use $\sigma_{\rm mt}^{\nu_i}$ to define such quantities as momentum transfer mean free path, collision frequency, and fractional energy loss per collision. On the other hand, the viscosity cross section, $\sigma_{\rm vi}^{\nu_i}$, is inversely related to the heat conductivity and viscosity of the gas or plasma. The weighting factor $\sin^2\theta$ in the viscosity cross section definition, which is maximum at $\theta = \pi/2$ and goes to zero for $\theta \longrightarrow 0$ or π, emphasizes the median region of the scattering angles. Collisions resulting in scattering to angles near $\pi/2$ are effective in inhibiting conductivity because they tend to equalize energy and thus lead to smaller viscosity and heat conduction.

3. Results

We have solved the coupled equations (12) for the ground electronic potential surface ($k = 0$) within a truncated set of vibrational states $0 \leqslant \nu \leqslant 9$, in the range of collision energies $0.1 \leqslant E \leqslant 100$ eV, for ten values of γ between 0 and $\pi/2$ (for $\pi/2 \leqslant \gamma \leqslant \pi$, the amplitudes are symmetric to those in the first quadrant). The calculation was performed for ten energies per decade, i.e. $E = 10^{0.1j-1}$, $j = 0, 30$.

Checking the convergence as a function of the number of partial waves $\ell_{\rm max}$ required consideration of two principal criteria. All nine inelastic (vibrationally excited) channels were included in the calculation until the elastic channel probability stably reached a value of 0.999 99 (if it is repeated ten times for a succession of ℓ-values), defining the quantity $\ell_{\rm max}^{\rm inel}$. Except for the highest energies treated, this was far below the convergence in ℓ needed for the elastic channel: the elastic amplitude $S_0^{(\ell)}$ oscillates for a range of large values of ℓ until it reaches our adopted convergence criteria $(1 - {\rm Re}\,\{S_0^{(\ell)}\} \leqslant 10^{-5}$, repeated ten times in succession†). The value of $\ell_{\rm max}^{\rm el}$ depends on collision energy and on the reduced mass of the system. We show typical variations of these quantities in table 1 for the mass extremes of the ion–molecule and atom–molecule hydrogen systems. We also note that there is a weak dependence of $\ell_{\rm max}$ on the molecular orientation (γ).

Three additional numerical convergence parameters are important in the calculation. These are the minimum and maximum values of the reaction coordinate R, and the step size of the numerical mesh. In all cases $R_{\rm min} = 0.05$ au, while $R_{\rm max} = 40$ and 15 au for the ion–molecule and atom–molecule case, respectively. The step size was varied between 0.0001 and 0.001 au, depending on the energy of the system considered.

Considerable attention was paid to obtain reliable potential surfaces $E_j(R, \rho, \gamma)$. For the atom–molecule systems, only the ground (lowest in energy) potential surface was needed, which is not the case for the ion–molecule systems. In the latter, there is a strong avoided crossing [7–9] between the two lowest potential surfaces at $\rho \simeq 2.6$ au, for all $R >\sim 4.5$ au. This is a consequence of the fact that when $\rho > 2.6$ the $H^+ + H_2$ surface is above the charge

† The two conditions, $1 \geqslant |S_0^{(\ell)}|^2 \geqslant 1 - 10^{-5}$ and $1 \geqslant {\rm Re}\,\{S_0^{(\ell)}\} \geqslant 1 - 10^{-5}$ imply $|{\rm Im}\, S_0^{(\ell)}|^2 \leqslant 10^{-5}$, which was fulfilled in our calculations.

Table 1. Typical values of the maximum angular momentum quantum number required to reach numerical convergence of the elastic scattering amplitude at $\gamma = 60^\circ$ with respect to the inelastic and pure elastic channels.

System	$H^+ + H_2$		$T^+ + H_2$		$H + H_2$		$T + T_2$	
E (eV)	ℓ_{max}^{inel}	ℓ_{max}^{el}	ℓ_{max}^{inel}	ℓ_{max}^{el}	ℓ_{max}^{inel}	ℓ_{max}^{el}	ℓ_{max}^{inel}	ℓ_{max}^{el}
0.1		56		90		42		68
1	41	153	80	257	17	98	38	183
5	152	326	277	561	144	191	255	358
10	251	455	443	787	209	216	367	472
100	1189	1314	2168	2406	649	649	1132	1132

transfer surface $H + H_2^+$ when $R \to \infty$. That is, when $R \to \infty$ the $H^+ + H_2$ surface becomes a function of only the diatomic coordinate ρ, $(H^+ + H_2)(R \to \infty, \rho, \gamma) \longrightarrow H_2(\rho)$, whereas $(H + H_2^+)(R \to \infty, \rho, \gamma) \longrightarrow H(1s) + H_2^+(\rho)$, the two ρ-dependent asymptotic triatomic curves cross at $\rho \approx 2.6$ au. Thus if the neutral molecule is in a high enough ($v \geqslant 4$) vibrational state, upon the approach of the projectile H^+ to the H_2 target, an almost diabatic transition is made to the lower adiabatic surface. To account for the effect of this triatomic surface avoided crossing 'seam' we transformed equations (9) for the two lowest H_3^+ adiabatic surfaces into the diabatic representation, following Baer [7,8]. The resulting diabatic potential surface that corresponds to $H^+ + H_2$ was then used for the ground surface in the reduced equations (equations (12)).

We have calculated the adiabatic surfaces for the ground state and the first excited state of H_3^+ utilizing a 54-state (11s, 6p) Gaussian basis in the unrestricted Hartree–Fock (full) configuration interaction (UHF-CI) approach using GAMESS [20]. The calculation was performed on a numerical mesh with a 0.1 au step† in ρ between 0.2 and 6 au and in R between 0 and 15 au, and for diatomic orientation angles $\gamma = 0$, 10, 20, 30, 40, 50, 60, 70, 80, 90°, and taking advantage of the fact the symmetry about $\gamma = 90^\circ$. At larger R we approximated the potential with dipole and polarization corrections. The surfaces were compared with the calculations of Ichihara [9] (who used a larger basis but in a narrower range of coordinates), and agreement was found to within 1.5% for the ground state (lower) surface. The adiabatic–diabatic transformation was performed using the nonadiabatic radial matrix elements determined by the diatom-in-molecule (DIM) method (see, e.g., [7]). This approach is quite accurate for values of R larger than 2 au (i.e. for R even smaller than value for which the 'seam' of avoided crossings occurs).

In treating the $H + H_2$ collisions problems emerge due to the high degree of symmetry present in the atom–diatom system. This is reflected in difficulties in calculating even the ground adiabatic potential surface accurately. We used the same basis as in the $H^+ + H_2$ case to calculate the ground potential surface for R, $\rho \leqslant 1$ au, for various γ using the UHF-CI method. This is then smoothly continued to the excellent analytical surface fit of Boothroyd [21], for $R \leqslant 10$ au, and continued for $R \geqslant 10$ au with an analytic asymptotic potential of the van der Waals type [10,11].

In both ion–molecule and atom–molecule cases, the R-dependent matrix elements, equation (9), were fitted using cubic splines for each fixed value of γ, and in that form used in the process of solving equations (12). The vibrational wavefunctions for H_2 of all vibrational states were found by numerical solution of the radial Schrödinger equation, equation (7), for vibrational quantum numbers $0 \leqslant v \leqslant 9$. This truncated vibrational basis containing

† Values for the potentials on the much finer numerical mesh were obtained by cubic spline interpolation.

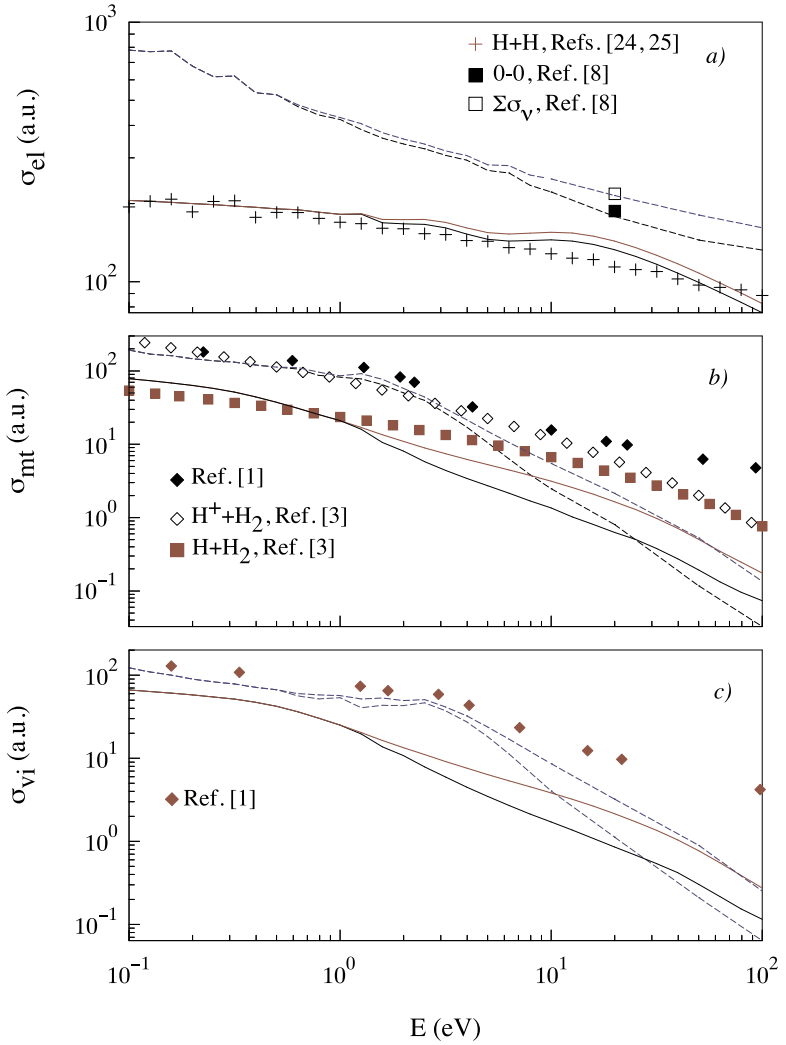

Figure 1. Integral (*a*) elastic, (*b*) momentum transfer, and (*c*) viscosity cross sections for scattering of H (solid curves) and H^+ (dashed curves) on H_2 in the ground vibrational state. In each case the lower curve is for $\nu_i = \nu_f = 0$ whereas the upper curve represents the sum over final vibrational states as described in the text. Comparison is made with previously existing results as noted in the figure.

nine excited vibrational states was enough to achieve acceptable accuracy for the elastic cross section on the ground vibrational state as well as for the excitation cross sections up to $\nu = 3$.

Figure 1 shows our results for the integral elastic, momentum transfer, and viscosity cross sections for scattering of H^+ and H on the ground vibrational state of H_2. For elastic cross sections we present both results for scattering on the ground vibrational state and summed over the vibrational excitation (i.e. $\sum_{\nu_f=1}^{9} \sigma_{el}^{\nu_f,0}$). For $H^+ + H_2$ we find an excellent agreement with the values given by Baer [8] at 20 eV. He calculated these cross sections by solving the Schrödinger equation numerically within the IOSA with full inclusion of vibrational motion on both the H_2 and H_2^+ surfaces, thus including charge transfer. The major approximation made by Baer is the DIM approximation for both ground and excited potential surfaces of

H_3^+ as well as for the nonadiabatic couplings. Nevertheless, comparison of his differential cross sections for vibrational excitation and for vibrationally resolved charge transfer with experimental results [15] indicates that the DIM approximation at 20 eV collision energy describes correctly the important parts of the potential surfaces and interactions. No data in the energy range considered are available for comparison with our results for $H + H_2$. We note that the vibrationally summed cross section does not deviate more than 10% from the one on the ground vibrational state.

In the energy range considered, since the elastic differential cross section is strongly peaked in the forward direction, the momentum transfer cross section is always significantly smaller than the integral elastic cross section. For $H+H_2$ the data available for comparison with our results are those recommended by Phelps [3] for the momentum transfer cross section, obtained by interpolation of the measured data of Lynch and Michael [22] at about 0.1 eV and theoretical data of Newman *et al* [23] for energies above 500 eV. For collision energies below 1 eV the Phelps data are in good agreement with ours (within 20%). At higher energies, where vibrational excitations become important, depleting the ground state, the Phelps data overestimate ours by up to one order of magnitude. Somewhat improved agreement is obtained if we sum momentum transfer cross sections over all vibrational states, thus defining the cross section for scattering on the ground electronic surface.

Phelps also derived a recommended curve for the momentum transfer cross section for $H^+ + H_2$ collisions in the range of energies $0.067 \leqslant E \leqslant 6670$ eV. The only data contributing to that recommendation that were obtained from experiments (on ion mobility) are for $E < 2.3$ eV. These data were then interpolated up to the cross sections of Smith *et al* [4], obtained for energies above 330 eV. As discussed by Phelps, the resulting curve is about an order of magnitude above the quantum mechanical calculations of Giese and Gentry [10] for energies of a few tens of eV. Our curve for scattering on the ground vibrational state is in good agreement with that of Phelps in the range of the measured data (below 3 eV). At the lowest energies, below 0.2 eV, this curve slightly diverges from our result. At high energies the Phelps curve is more than an order of magnitude above our results and about five times above our momentum transfer cross section summed over vibrationally excited states. The classical calculations of Bachmann and Reiter [1], which do not take into account the vibrational structure of H_2, overestimate the Phelps curve at high energies by almost an order of magnitude, but agree with both Phelps and our curve at lower energies, where vibrational excitation is negligible.

We expect that in the gap between the data used by Phelps there is a steeper decline of the momentum transfer cross section, caused by the regime of strong and resolvable vibrational excitations. The fact that we have not taken into account the vibrational states of the charge transfer channel does not influence the conclusion. This would effectively increase the number of excited vibrational states and thus make the minimum even deeper. Phelps also drew several qualitative conclusions regarding the behaviour of the momentum transfer cross section that are consistent with our results. For example, he noted that at high energies (about 100 eV), the cross sections for both H and H^+ scattering on the ground electronic surface of H_2 approach each other, reflecting simply the size of the target H_2 molecule, averaged and appropriately weighted over all excited vibrational states.

Figure 1(*c*) displays our results for the viscosity cross section compared with the classical results of Bachmann and Reiter [1]. Unlike the elastic cross section (not shown in this figure), the momentum transfer and viscosity cross sections in classical calculations are not dependent on the choice of an arbitrary cut-off parameter that is required to make the cross section finite. Thus, the cross sections are in reasonable agreement with our results up to several eV. Beyond this energy, they remain too large, similar to the behaviour of the classical momentum transfer cross section since, among other differences, the classical calculation does not take into account

any vibrational structure of the molecular target. As for the momentum transfer cross section, the viscosity cross sections summed over v_f for both H^+ and H projectiles almost coincide at the high end of the energy range.

We note that, in general, both the elastic cross section and its transport moments are larger for H^+ than H projectiles at lower energies. This is especially pronounced for the elastic cross section since it is dominated by the small scattering angles and thus, large impact parameters, where the differences between the polarization (for H^+) and van der Waals potentials (for H) are strong. The differences are smaller in the momentum transfer and viscosity cross sections, since these are dominated by the behaviour at large scattering angles, where the target properties dominate the character of the scattering during the close approach of the projectile.

It is also very interesting to note the striking similarity of the elastic cross sections for $H + H_2$ and H+H, also shown in figure 1(*a*). This implies that the basic physical mechanism in scattering of H on H_2 is the interaction of the incident atom with the nearest atom of the molecule. In contrast, the well established mechanism for excitation, and thereby for the intimately connected elastic scattering of H^+ on H_2, is the effect of 'bond dilution,' as discussed in the introduction. Due to the long-range polarization forces, absent in the $H + H_2$ case, the proton acts simultaneously with both atoms in the molecule, causing a maximal contribution from scattering when the molecular orientation is almost perpendicular to the incident direction. To support this conclusion, we show in figure 2 the integral cross sections weighted by the factor $\sin\gamma$ that is used to average over molecular orientations (see equation (14)), for both the elastic and first two vibrational excitations of H_2. These are shown as functions of γ, for various collision energies. For $H^+ + H_2$, the maximum contribution to the averaged cross section indeed tends to come from large values of γ, for both the elastic and inelastic cross sections. In contrast, for the $H + H_2$ case, contributions to the cross section tend to minimize at the largest values of γ. It comes predominantly from the nearly collinear geometries, where the interaction of the projectile with individual atoms in the molecule dominates.

A comparison between our differential cross sections for elastic scattering of H and H^+ on the ground vibrational state of H_2 is shown in figure 3 for several collision energies. The other available theoretical data for $H^+ + H_2$, that of Schinke *et al* [11, 12] and Baer *et al* [8], and the experimental data of Hermann *et al* [14] and Niedner *et al* [15], show good agreement with our fully quantal calculations. Both the Schinke *et al* and Baer *et al* calculations were performed using the IOSA approximation. Some deviations from our results toward small scattering angles in the Baer calculation can be explained by the insufficient number of angular momenta Baer used (about 250 compared to about 600 that we found to be needed for convergence of the elastic amplitudes at a collision energy of 20 eV). The deviations at larger scattering angles might be attributed to inaccuracy of the DIM potentials at small internuclear distances. The pronounced rainbow in the $H^+ + H_2$ cross sections is not present in the $H + H_2$ cases. A small structure is present in the latter case, for smaller angles. In both cases the rainbow flattens and moves toward smaller angles with increase of the collision energy, as expected. At the smallest scattering angles, the H^+ scattering has a larger cross section than that for H scattering, due to the presence of the polarization potential in the former case.

The elastic, momentum transfer, and viscosity cross sections for scattering of H and H^+ on the three lowest vibrationally excited states of $H_2(v_i)$, $v_i = 1, 2, 3$ are shown in figure 4. A general characteristic of the elastic cross sections for $v_i > 0$ is that they are somewhat larger that the one on the ground state and that they show a sudden drop in the region in which vibrational excitation becomes significant. The momentum transfer and viscosity cross sections are somewhat smaller than the corresponding quantities for $v_i = 0$. In most of the cases, the largest cross sections are those for $v_i = 1$, and there is continuous decrease with increase of v_i. All these features are a consequence of the competition between the varying

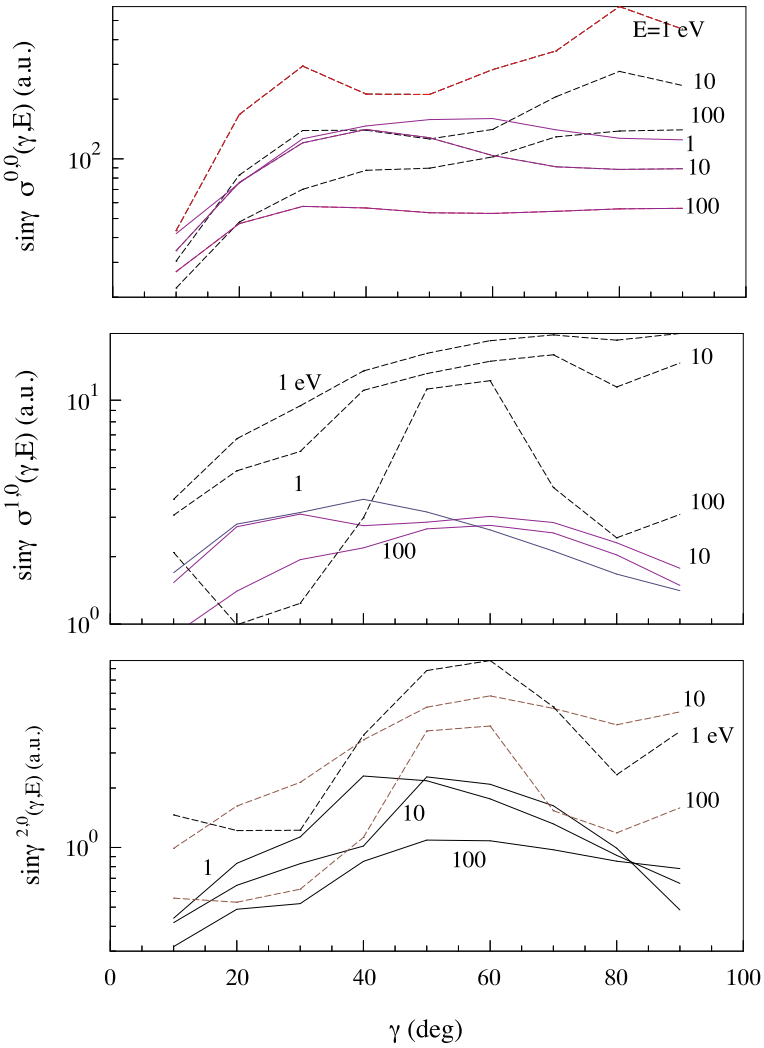

Figure 2. Contributions from various H_2 orientations, γ, to the integral (*a*) elastic, (*b*) excitation into $v_f = 1$, and (*c*) excitation into $v_f = 2$ cross sections for scattering of H (solid curves) and H^+ (dashed curves) on H_2 initially in the ground vibrational state for various centre of mass collision energies.

size of the target (i.e. the spatial size of the electronic wavefunction increases with increasing v_i) and the change in the 'bond dilution' effect on one hand, and of the role and degree of vibrational excitation and deexcitation on the other.

Figure 5 illustrates the behaviour of the integral cross sections as a function of collision energy for vibrational excitation in $H + H_2$ and $H^+ + H_2$ collisions, starting from the ground vibrational state ($v_i = 0$). In the former case, although the elastic cross section is almost two orders of magnitude larger, the inelastic cross sections for various v_f are closer to one another at higher energies, with the obvious dominance of the $v_f = 1$ case. For each v_f, the cross section has its maximum for energies above its respective threshold, but decreases after the next v_f -channel is open, resulting in a local minimum of the $(v_f - 1)$-channel. Qualitatively,

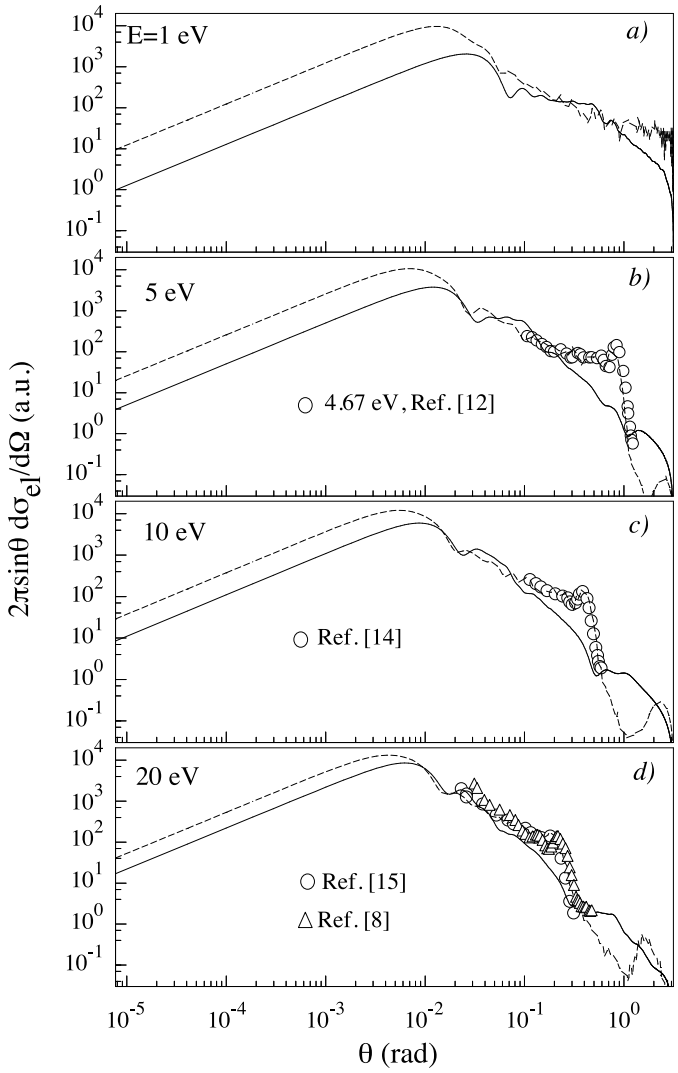

Figure 3. Differential elastic cross sections for scattering of H (solid curves) and H^+ (dashed curves) on H_2 in the ground vibrational state for different collision energies. Comparison is made with existing results as noted in the figure.

a similar behaviour of the excitation cross sections is displayed by the results for the $H^+ + H_2$ system, the differences being attributed to the varying basic mechanisms of excitation in the two systems. That is, the principal excitation mechanism for ion impact is the perturbation of the electronic distribution of the molecule by the proton, which may extend to large values of the reaction coordinate, while for atom impact, the direct collision of the projectile with the closest atom in the molecule is mainly responsible for the reaction. As a consequence, for $H^+ + H_2$ in the threshold region, the cross sections reach their maxima much faster and obtain somewhat larger values. Also regarding the $H^+ + H_2$ system, the differences between the cross sections for different v_f are also larger, but with obvious dominance of the $v_f = 1$ case at larger energies.

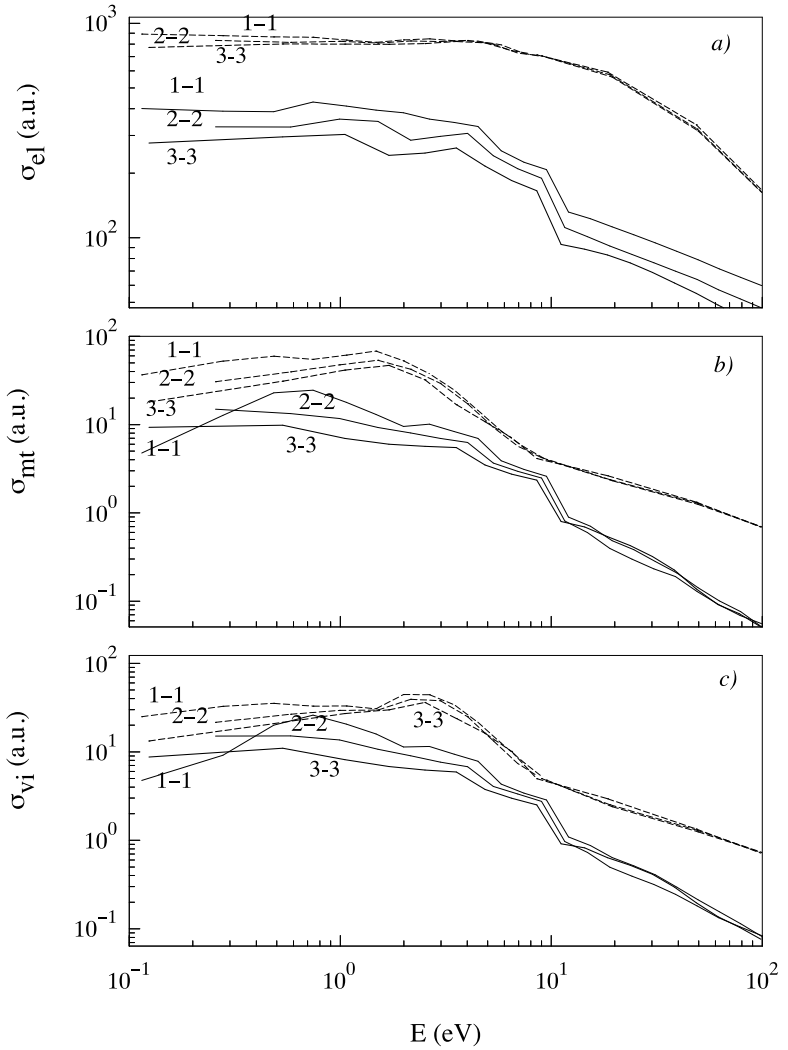

Figure 4. Integral (*a*) elastic, (*b*) momentum transfer, and (*c*) viscosity cross sections for scattering of H (solid curves) and H^+ (dashed curves) on H_2 initially in the first three excited vibrational states. The symbols indicate the initial and final vibrational level of H_2.

Also in figure 5, we compare our results for $H^+ + H_2$ elastic and inelastic collisions with those available in the literature and note that we are not aware of any available data for $H + H_2$. The agreement of our fully quantal calculations with the other data is good at all energies for the elastic and first excited state, but deteriorates with decreasing collision energy and increasing of values of ν_f. Since all of the results displayed, including the present one, have been performed using the IOSA, the disagreement might be attributed to the absence of H_2^+ vibrational states in our calculations which might influence the distribution of excited states at higher energies. It might also be attributed to the use of imprecise analytically fitted electronic surfaces in the works of Giese and Gentry [10] and Schinke *et al* [12, 13], in the use of the classical DECENT approach defined by and used by Giese and Gentry [10], in the use of the straight-line trajectory method by Schinke *et al* [13], and in the inadequacy of the DIM

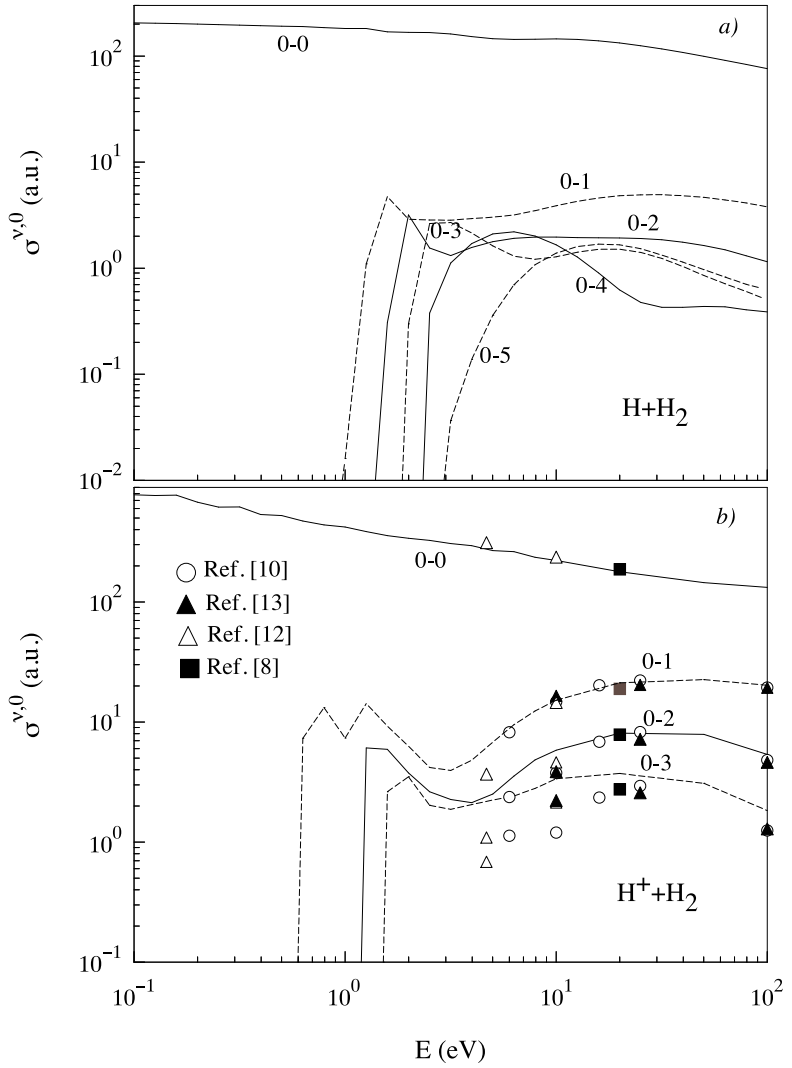

Figure 5. Integral cross sections for vibrational excitation in scattering of (*a*) H on H_2 and (*b*) H^+ on H_2 initially in the ground vibrational state. The solid and dashed curves alternate as a function of final vibrational state to aid the clarity in this figure for both H and H^+ impact. Comparison is made with existing data as noted in the figure.

electronic surfaces at small internuclear distances [8].

Comparison among our differential cross sections for vibrational excitation from $H_2(v_i = 0)$ to $H_2(v_f = 1, 2, 3)$ by H and H^+ impact at a collision energy of 10 eV is presented in figure 6. Also shown is that the present $H^+ + H_2$ results are in good agreement with the absolute experimental data of Hermann *et al* [14] for various v_f. This occurs despite the poor agreement for $v_f = 2, 3$ with other theoretical integral vibrational excitation cross sections at lower energies (figure 5(*b*)). An obvious characteristic of the inelastic cross sections displayed compared with the elastic cross section is the dominance of the large scattering angles, reflecting the role of the small impact parameters in vibrational excitation. The pronounced rainbow at $\theta \sim 0.4$ rad for the $H^+ + H_2$ system is mainly responsible for the larger values of the excitation

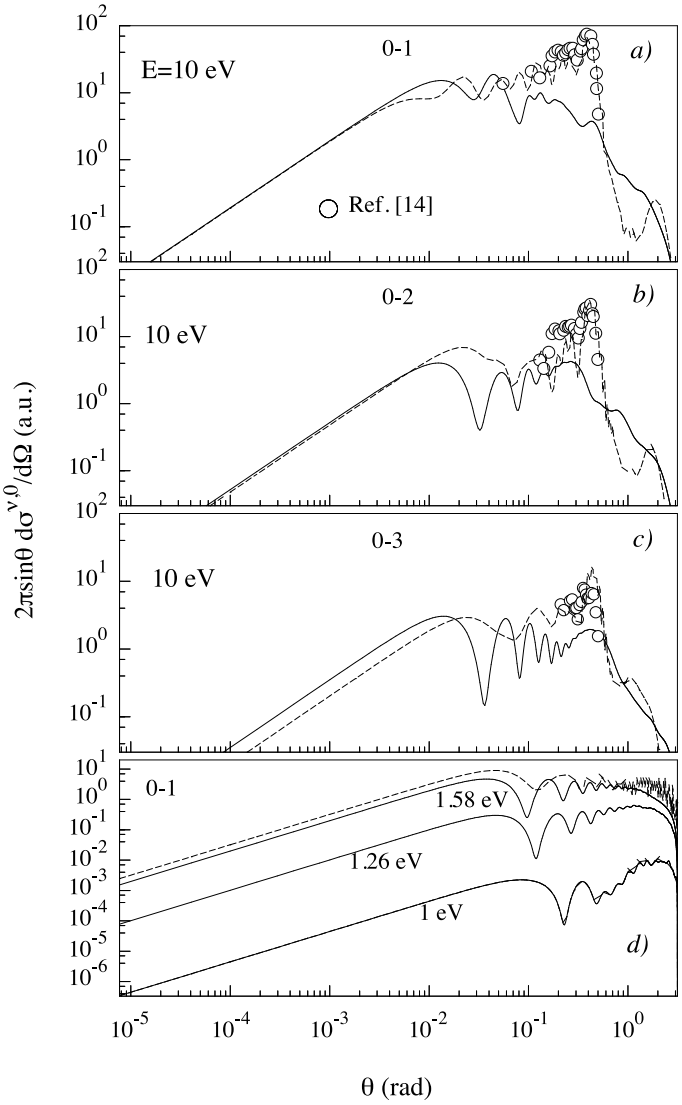

Figure 6. Differential cross sections for vibrational excitation of H_2 in scattering with H (solid curves) and H^+ (dashed curves). Comparison is made with the absolute experimental measurements of Hermann *et al* [14]. (*a*) 10 eV, 0–1, (*b*) 10 eV, 0–2, (*c*) 10 eV, 0–3, and (*d*) 1, 1.26, and 1.58 eV, 0–1 (energies near threshold).

cross sections in comparison to the $H + H_2$ case. Figure 6 also shows the behaviour of the differential cross sections for $H + H_2$ for several energies close to, but above, the first excitation threshold ($v_f = 1$). For $E \sim 1.58$ eV we note that the differential cross section almost coincides with the corresponding cross section for the $H^+ + H_2$ case. For lower energies, the curves representing the differential cross section shift in a parallel fashion toward larger values with increase of energy.

4. Conclusions

We have presented the first comprehensive study of elastic scattering of H on H_2 in the range of centre of mass collision energies of 0.1–100 eV, based on fully quantal calculations and with the inclusion of vibrational excitation only, while rotational dynamics is treated within IOSA. In the absence of a pre-existing, benchmarking calculations, we have also treated the elastic and vibrationally inelastic scattering of H^+ on H_2, favourably comparing with the data available in literature for this system. In addition, due to their utility for plasma modelling, transport cross sections as well as scattering on excited vibrational states have also been calculated. We have found that the vibrational excitation cross sections for the $H + H_2$ system display features not present for $H^+ + H_2$ collisions. The dominant scattering mechanism for $H + H_2$ is identified as scattering of the projectile on the closest atom in molecule, in contrast to the $H^+ + H_2$ system, where both elastic scattering and vibrational excitations are governed by perturbation of the electronic distribution of the molecule by the passing proton.

We note that an analysis and description of the relevant scaling of the integral cross sections for scattering of H and H^+ on H_2 in various isotopic combinations (H^+, D^+, T^++H_2, D_2, DT, ...) is presented elsewhere [24], as are fitting coefficients for all of the differential and integral cross sections for ease of use in plasma modelling applications [25]. The calculated data for differential and integral cross sections discussed in this paper, as well as those for the various isotopic combinations, can be viewed and downloaded from the web site of the Controlled Fusion Atomic Data Center at Oak Ridge National Laboratory, `www-cfadc.phy.ornl.gov`.

Acknowledgments

This work has been supported by the US Department of Energy, Office of Fusion Energy Sciences, at Oak Ridge National Laboratory which is managed by Lockheed Martin Energy Research Corporation under contract No DE-AC05-96OR22464.

References

[1] Bachmann P and Reiter D 1995 *Control Plasma Phys.* **35** 45
[2] Janev R K (ed) 1995 *Atomic and Molecular Processes in Fusion Edge Plasmas* (New York: Plenum)
[3] Phelps A V 1990 *J. Phys. Chem. Ref. Data* **19** 653
[4] Smith K A, Johnson L K, Gao R S and Stebbings R F 1987 *Abstracts of Contributed Papers for the Int. Conf. on the Physics of Electronic and Atomic Collisions* ed J Geddes *et al* (Amsterdam: North-Holland) p 681
[5] Forrey R C, Balakrishnan N, Dalgarno A and Lepp S 1997 *Astrophys. J.* **489** 1000 and references therein
[6] Baer M and Nakamura H 1987 *J. Chem. Phys.* **66** 1363
[7] Baer M, Niedner G and Toennies J P 1988 *J. Chem. Phys.* **88** 1461
Baer M 1992 *State-Selected and State-to-State Ion–Molecule Reaction Dynamics, Part 2: Theory (Advances in Chemical Physics vol LXXXII)* ed M Baer and C-Y Ng, p 187
[8] Baer M, Niedner-Schatteburg G and Toennies J P 1989 *J. Chem. Phys.* **91** 4169
[9] Ichihara A and Yokoyama K 1995 *J. Chem. Phys.* **103** 2109
[10] Giese C F and Gentry W R *Phys. Rev.* A **10** 2156
[11] Schinke R, Dupuis M and Lester A Jr 1980 *J. Chem. Phys.* **72** 3909 and references therein
[12] Schinke R and McGuire P 1978 *Chem. Phys.* **31** 391
[13] Schinke R 1977 *Chem. Phys.* **24** 379
[14] Herman V, Schmidt H and Linder F 1978 *J. Phys. B: At. Mol. Phys.* **11** 493
[15] Niedner G, Noll N and Toennies J P 1987 *J. Chem. Phys.* **87** 2685
[16] Monchick L and Mason E A 1961 *J. Chem. Phys.* **35** 1676
[17] Kouri D J 1979 *Atom Molecule Collision Theory* ed R B Bernstein (New York: Plenum)
[18] McDaniel E W 1964 *Collision Phenomena in Ionized Gases* (New York: Wiley)
McDaniel E W 1993 *Atomic Collisions: Heavy Particle Projectiles* (New York: Wiley)

[19] Johnson B R 1973 *J. Comput. Phys.* **13** 445
[20] Schmidt M W *et al* 1993 *J. Comput. Chem.* **14** 1347
[21] Boothroyd A I, Keogh W J, Martin P G and Peterson M R 1991 *J. Chem. Phys.* **95** 4343
[22] Lynch K P and Michael J V 1978 *Int. J. Chem. Kin.* **10** 233
[23] Newman J H, Chen Y S, Smith K A and Stebbings R F 1986 *J. Geophys. Res.* **91** 8947
Newman J H, Chen Y S, Smith K A and Stebbings R F 1989 *J. Geophys. Res.* **94** 7019
[24] Krstić P S and Schultz D R 1999 *Phys. Rev.* A submitted
[25] Krstić P S and Schultz D R 1998 Atomic and plasma-material interaction data for fusion *Nucl. Fusion (Suppl.)* **8**